

AMPLITUDE-INDEPENDENT MACHINE LEARNING FOR PPG THROUGH VISIBILITY GRAPHS AND TRANSFER LEARNING

Yuyang Miao, Harry J. Davies, Danilo P. Mandic

Imperial College London

ABSTRACT

Photoplethysmography (PPG) signals are omnipresent in wearable devices, as they measure blood volume variations using LED technology. These signals provide insight into the body’s circulatory system and can be employed to extract various bio-features, such as heart rate and vascular ageing. Although several algorithms have been proposed for this purpose, many exhibit limitations, including heavy reliance on human calibration, high signal quality requirements, and a lack of generalization. In this paper, we introduce a PPG signal processing framework that integrates graph theory and computer vision algorithms, which is invariant to affine transformations, offers rapid computation speed, and exhibits robust generalization across tasks and datasets.

Index Terms— Photoplethysmography (PPG), Visibility Graph, Transfer Learning, Graph Theory

1. INTRODUCTION

Photoplethysmography (PPG) sensors are widely employed in wearable devices due to their non-invasive and portable nature. Through estimation of blood volume at the site of the probe, PPG can be used to estimate heart rate, respiration, blood pressure, vascular stiffness and much more. A wide range of applications work on PPG signals including, but not limited to, cognitive load classification [1, 2], blood glucose monitoring [3, 4] and Chronic obstructive pulmonary disease (COPD) diagnosis [5].

Numerous studies have focused on extracting respiratory information from PPG signals [6, 7, 8]. Motin *et al.* [9] utilized Empirical Mode Decomposition (EMD) and its variations to decompose PPG signals into their components. The authors then selected the Intrinsic Mode Functions (IMFs) devoid of artefacts and heart rate information, and applied the Principal Component Analysis (PCA) algorithm to the remaining components to extract respiratory rates. Madhav *et al.* [6] proposed using Multi Scale Principal Component Analysis (MSPCA) for respiratory envelope extraction. Multiple periods of PPG signals were concatenated to form a matrix, with each row representing one period of the PPG signal. Wavelet transform was performed on each row, resulting in a matrix of wavelet coefficients. The coefficients were adjusted

based on statistical features and processed through a PCA algorithm to obtain the final breathing envelope.

PPG signals can also be utilized to estimate vascular ageing. Dall’Olio *et al.* [10] proposed an algorithm for vascular ageing classification using PPG signals. They initially removed the trend in the PPG signal using a centered moving average. The processed PPG signal was then demodulated using a Hilbert transform, and the envelope was extracted. The final version of the PPG signal was obtained by dividing the demodulated signal by the envelope. A recursive peak detection method was subsequently applied to extract windows of 15 peaks, which were fed to a ResNet module for binary vascular ageing prediction. Additionally, a Support Vector Machine (SVM) model was constructed using features from metadata and features extracted from the PPG signals.

In 2009, Suzuki and Oguri conducted pioneering work combining machine learning and blood pressure prediction [11]. The study utilized physiological features, including Pulse Width (PW), Transit Time (TW), Dicrotic Wave (DW), and Dicrotic Notch (Dn). An AdaBoost model was trained to predict systolic and diastolic blood pressures.

These algorithms have demonstrated strong performance, however, several limitations prevent their more widespread use in practice. These include:

- A considerable amount of preprocessing based on manually designed rules is required, such as a manual selection of intrinsic mode functions.
- Existing algorithms are sensitive to parameter choice and may not generalise well across different datasets.
- The majority of approaches employ the magnitude of the PPG signal as an input feature, which can be easily influenced by factors such as age, skin thickness, and skin tones.
- Numerous methods directly work with features extracted from temporal domain PPG signals, making them highly sensitive to signal quality and effects of affine transformations.
- Many existing solutions necessitate complex feature extraction operations.

To address these issues, we propose an algorithm that combines the visibility graph and transfer learning techniques. By virtue of the visibility graph approach, the time series of the PPG signal is transferred into a complex graph network which preserves the structural information while discarding the magnitude information. This provides an opportunity to create visibility graphs and use their adjacency matrices in the context of transfer learning, which has demonstrated robust performance in areas such as computer vision. This joint treatment of graphs and transfer learning offers several advantages:

- Robustness to affine transformations by virtue of the visibility graph.
- Use of only geometric information in the PPG signal, making the approach amplitude-independent.
- Minimal preprocessing requirements.
- Fast computation speed.
- Good generalisation across different tasks and datasets.

This work is structured as follows: In Section 2, we introduce the proposed algorithm and outline the visibility graph and transfer learning techniques. In Section 3, we conduct experiments on two publicly available datasets using the proposed algorithm, demonstrating its generalisability in both tasks and datasets. Finally, in Section 4, we present conclusions discussing the performance and future directions.

2. METHODOLOGY

2.1. Signal To Graph: Visibility Graph

A graph $G = V, E$ is defined by a set of vertices V connected by a set of edges E . Figure 1a illustrates a graph where the vertices are represented as dots, and the lines connecting them are the edges of the graph. The horizontal black line acts as an axis for the dots. For simplicity, all graphs in this work are undirected, which means that all edges are bi-directional. The visibility graph transforms a time series into a graph [12], whereby each signal sample y_i is considered to be a vertex. There is an edge connecting two vertices if there exists a line connecting these two signal points which does not intersect with another signal point; this can be interpreted as one signal sample seeing another one without a third signal sample blocking them. More formally, two vertices, y_a and y_b , are connected by an edge if

$$y_c < y_b + (y_a - y_b) \frac{t_b - t_c}{t_b - t_a} \quad (1)$$

for any other signal sample y_c . Since we consider undirected graphs, all visibility is mutual, which means y_b can see y_a if y_a can see y_b . Figure 1b gives an example of the transformation from a time series signal to a visibility graph.

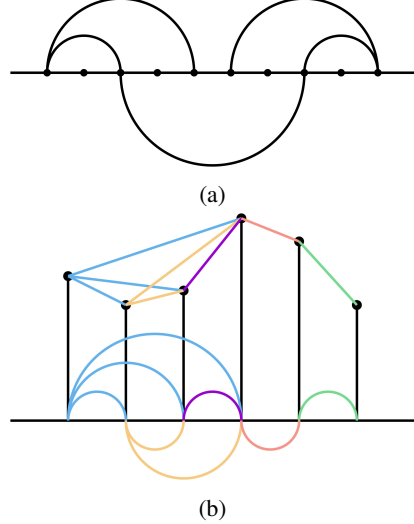


Fig. 1: From a time series to a visibility graph. (a) A simple graph with nodes (dots) and edges. (b) An example of a visibility graph. The vertical stems represent the signal, while the curved lines represent edges connecting the corresponding visibility graph vertices.

2.2. Graph To Image: Adjacency Matrix

The adjacency matrix is used to describe the connectivity of a graph. For a graph with N vertices, an adjacency matrix A has a size of $N \times N$. For a weighted graph, if two vertices V_i and V_j are connected, then $A_{i,j} = w_{i,j}$, while $A_{i,j} = 0$ if not connected. The weight $w_{i,j}$ may be calculated using some specific rules, for example, distance, correlation, etc. For an unweighted graph, $w_{i,j}$ will always be unity or zero. Note that the adjacency matrix can be considered as a grayscale image and a black-and-white image for weighted and unweighted graphs, which is suitable as input to a 2D convolutional neural network. Figure 2 gives an example of a time series signal, an unweighted graph generated from the signal, and its corresponding adjacency matrix, viewed as both a matrix and an image. Our proposed framework operates specifically with the adjacency matrix of the visibility graph. To this end, the time series PPG signal is first transformed into visibility graphs and then transformed into images in the form of adjacency matrices.

2.3. Visibility Graph: Invariant To Affine Transformation

The visibility graph is invariant to affine transformations; in other words, the visibility graph is invariant to the horizontal or vertical scaling of the original signal. Figure 3 provides an example, whereby the original signal, is moderately and heavily affine transformed, Observe that even heavily affine transformed signals have precisely the same visibility graph and the same adjacency matrix.

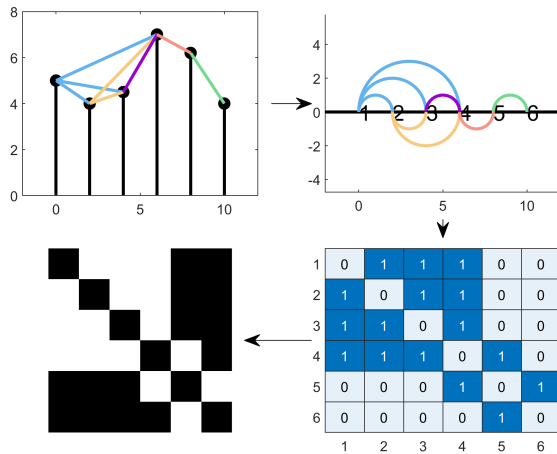


Fig. 2: Pathway from a time series to an image: The original signal and the visibility between signal samples (top left). The visibility signal generated from the input signal (top right). The adjacency matrix corresponds to the visibility graph (bottom right). The black-and-white image that generated from the adjacency matrix (bottom Left).

2.4. The PPG signal as a Visibility Graph

We now demonstrate the effects of various breathing patterns, heart rates, and age on the adjacency matrices of visibility graphs of the corresponding PPG signals. The examples show that a visibility graph can capture the structural characteristics of PPG signals, providing a foundation for further analysis. These results suggest that visibility graphs could potentially be used to analyse PPG signals and extract important physiological information.

2.4.1. Breathing Modulation

The PPG signal, a quantification of changes in blood volume through the absorbance of light, is subject to modulation by alterations in respiratory patterns. These modulations stem from variations in venous return, stroke volume, tissue volume, and respiratory sinus arrhythmia [13, 5]. The impact of respiratory activity modulation on PPG signals can be categorised into three distinct groups: amplitude modulation (AM), baseline wandering (BW), and frequency modulation (FM). Notably, BW modulation, which arises from fluctuations in venous pressure, is the most readily discernible characteristic within the raw PPG signal [5].

To investigate the effects of deep breathing on the PPG signal, we conducted an experiment whereby a subject initially breathed normally and then commenced deep breathing. Figure 4 depicts the resulting PPG signal segments and their corresponding adjacency matrices. Observe the BW modulation, a sinusoidal waveform shape, in the adjacency matrices.

This modulation introduced additional peaks that were not present in the normal PPG signal, thus giving certain pulses of the PPG signal additional visibility, which was manifested as white squares in the adjacency matrices.

2.4.2. Heart rates

An additional easily observable feature is the heart rate (HR). The PPG signal of the subjects was initially recorded at rest and subsequently after exercising. Figure 5 illustrates the differences in the adjacency matrices of the PPG segments with different heart rates. The wing-shaped elements along the diagonal signify peaks in the PPG signal. It is evident that the number of wing-shaped elements grows with heart rate, for a fixed window length.

2.4.3. Vascular Ageing

The shape of the PPG signal also varies with age, with the dicrotic notch less pronounced as age increases, yielding a smoother PPG signal [14]. Figure 6 offers an example of how the visibility graph can determine subjects' vascular ageing. The left side of the first row of Figure 6 depicts the PPG signal of a subject aged 13, while the right side displays a 49 years old subject. The second row presents the corresponding adjacency matrices, note that the adjacency matrices exhibit significant differences. For a younger subject, the PPG signal is less smooth and has more notches, leading the adjacency matrix to have more white pixels denoting that two nodes can see each other. Conversely, due to the smoothness of the PPG signal of the older subject, most of the data points cannot see each other, producing an image less filled with white.

In the previous section, we illustrated that physiological activities could be reflected in the adjacency matrices of the corresponding visibility graphs to a certain extent. We next introduce the concept of transfer learning and show how it can be applied to visibility graphs.

2.5. Transfer Learning

Deep learning has been successful in achieving impressive results in the field of computer vision. However, state-of-the-art models often require large amounts of data for training, leading to the issue of data dependence. Transfer learning offers a solution to this problem by training models on large datasets to obtain a set of pre-trained weights, which are then fine-tuned on smaller datasets. This significantly reduces the required amount of data and allows large deep learning models to be applied to a broader range of fields and scenarios [15]. Our study employed the VGG19 model for training, after conducting empirical tests. The VGG19 model is a Convolutional Neural Network (CNN) with 19 layers, comprising 16 convolutional layers and three fully connected layers. It is equipped with five maxpooling layers and a final Softmax activation function. Depending on the task at hand, the output

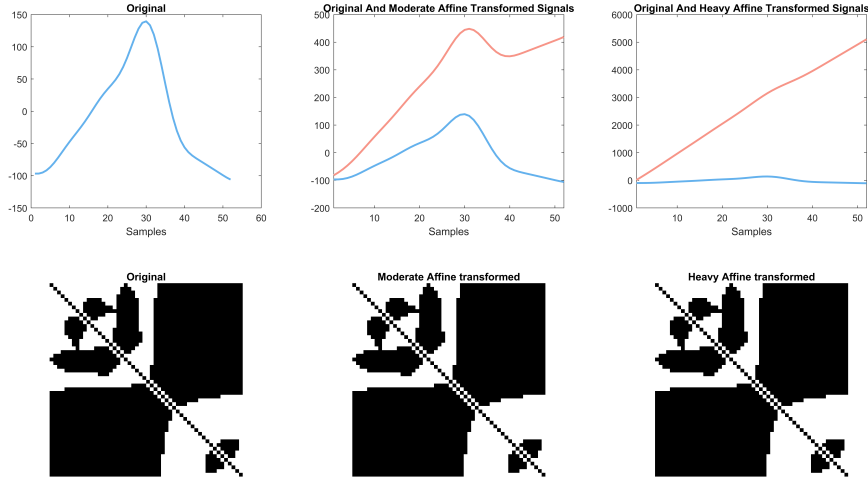


Fig. 3: Visibility graphs of PPG signals under moderate, heavy and no affine transformation. The adjacency matrices of these signals are identical, which demonstrates the amplitude-independence of the visibility graph domain.

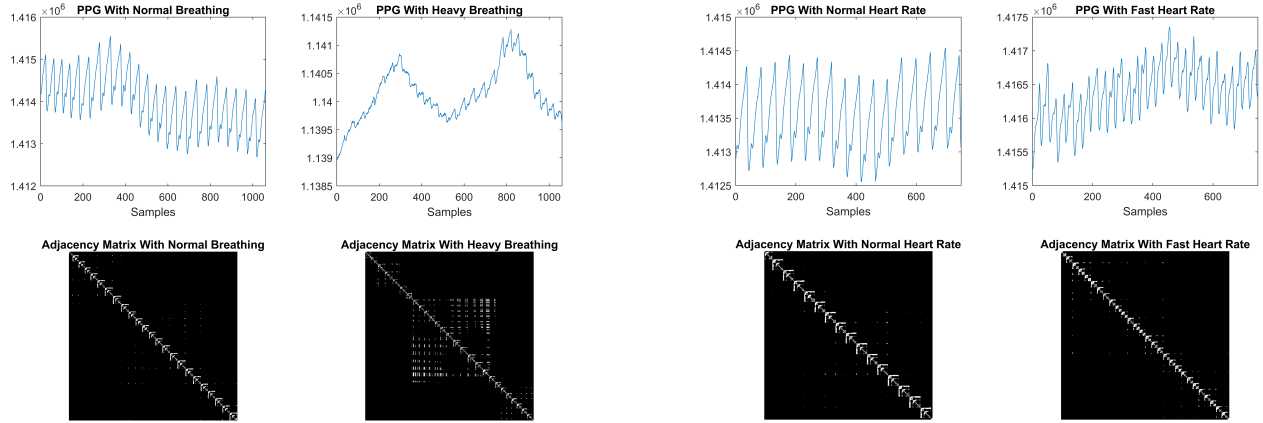


Fig. 4: Example PPG waveforms and the corresponding adjacency matrices of normal breathing (left) and deep breathing (right).

layer, which is the final fully connected layer, can be altered to meet the desired output dimension. The VGG19 model was initialised with weights trained on the ImageNet dataset [16].

2.6. Proposed Learning Scheme: VGTL

The proposed learning scheme termed VGTL (Visibility Graph and Transfer Learning) is capable of classification and regression tasks with arbitrary size. It comprises three steps: The PPG signal is segmented into a fixed-length window or a fixed number of pulses. The segmented PPG signals are

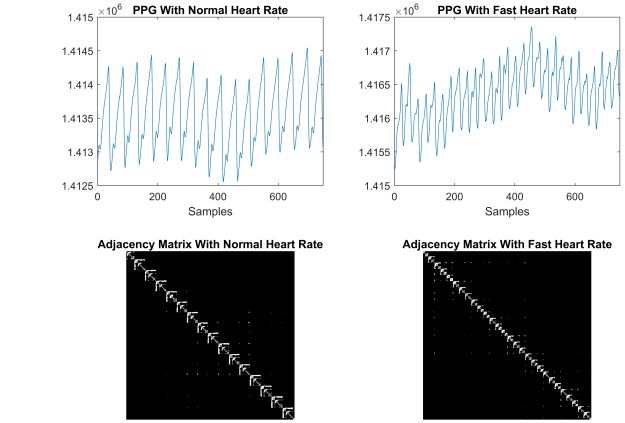


Fig. 5: Two segments of PPG signal with different heart rates (top panel) and their adjacency matrices generated from the visibility graphs (bottom panel).

then transformed into adjacency matrices and transformed into grayscale images. The adjacency matrix images are fed to the VGG19 algorithms to give the final output.

3. EXPERIMENTS AND RESULTS

We conducted two experiments to validate the proposed approach. The first experiment considered the prediction of vascular ageing, while the second experiment aimed to predict the systolic and diastolic blood pressure and the corresponding blood pressure waveforms.

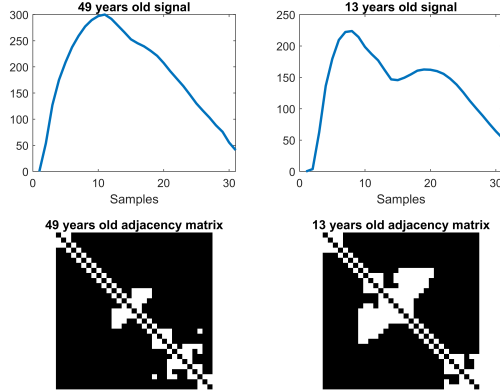


Fig. 6: Age related characteristics of PPG signals and the corresponding adjacency matrices. Left Panels: 49 years old subject Right Panels: 13 years old subject.

3.1. Vascular Ageing

3.1.1. Dataset

The dataset used for vascular ageing prediction was the "Real-World PPG Dataset" from Mendeley [17]. This dataset consists of PPG signals for 35 healthy subjects, with 50-60 PPG signals per subject. The duration of each PPG signal is 6 seconds, with a sampling rate of 50 Hz. The ages of subjects range from 10 to 75 years old. The dataset is divided into training, validation, and test datasets.

3.1.2. Aim and Goal

This experiment utilised the proposed VGTL scheme to predict the age of subjects based on their PPG signals. The prediction was conducted in the regression and classification settings. For the regression task, the VGTL aims to predict the exact age of the subject, while for the classification task, the VGTL aims to determine the age group of the subject, namely 0-20, 20-30, 30-40, and 40+.

3.1.3. Data Preparation and Model Architecture

The PPG signals were segmented into individual peaks, with every training, validation or test sample containing only one peak. As the heart rate can change between or even within subjects, an average length of 50 samples was selected (1 second). Segments longer than 50 samples were truncated, and those shorter than 50 were padded with zeros. Figure 7 illustrates such padding and truncation.

Next, the PPG pulses were transformed into visibility graphs, and the corresponding adjacency matrices were converted into images to feed the VGG19 model which was pre-trained on the ImageNet dataset. Figure 8 illustrates the

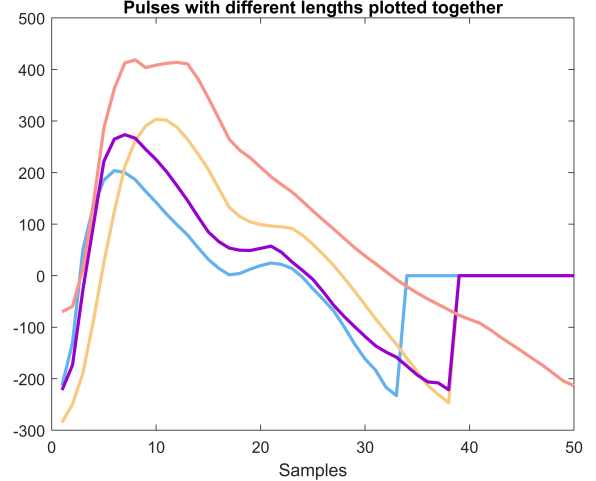


Fig. 7: PPG pulses of different lengths visualised in the same graph. Pulses longer than 50 data points are truncated and pulses shorter than 50 data points are zero-padded.

three-channel input system. The VGG19 model requires 3 channels of images; the inputs of the three channels were the adjacency matrix generated from the PPG pulses, the adjacency matrix generated from the inverted PPG pulses, and the adjacency matrix of a slope-weighted visibility graph generated from the inverted PPG signal. For slope-weighted visibility graphs, the edge weights, the non-zero values of the adjacency matrices, depend on the slope of the line connecting the two data points. Since the three channels were considered to be the RGB channels, Figure 9 shows an example of an input image of the VGG19 model. No preprocessing was required. The **findpeaks** function in **MATLAB** was used to extract pulses from the PPG signals. Then the adjacency matrices were shuffled and divided into the training, validation, and test sets with sizes of 10131, 2586, and 2586. Ten consecutive tests were performed using different training/validation/test distributions (different random seeds). The results were analysed by calculating the mean and standard deviation.

As for the model architecture, the VGG19 model was pre-trained on the ImageNet dataset with 1000 classes. Thus, a fully connected top layer with the size of 1000×4 and a Softmax activation function were added to the VGG19 model for the classification task. In addition, top layers of size 1000×1 and 1000×2 were included for the regression and binary classification task.

3.1.4. Results and Discussions

We compared our methods for the classification task with the one proposed by Dall'Olio *et al.* [10]. The original paper employed binary classification into the young and old. To make a fair comparison, we adopted the method in [10] to our dataset

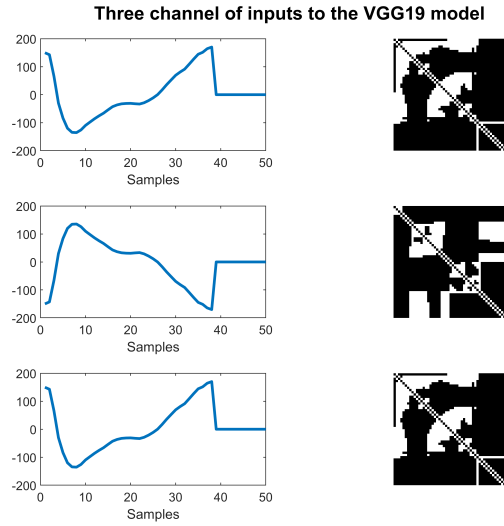


Fig. 8: Three channels of a PPG pulse (Left) and their corresponding adjacency matrices (Right).



Fig. 9: The RGB version of the input images.

for a four-class classification. We also applied our method to a binary classification task, classifying subjects into classes of below 30 and above 30 in age. For the four-class classification task, the work in [10] uses windows of 15 pulses which did not converge for our dataset. So our data segmented scheme, 50 signal samples per window, was employed instead of the original 15 peaks window scheme in [10]. For the training strategy, the learning rate at the beginning was 10^{-5} and decreased by a factor of 10 if the loss of the validation set did not decrease after 5 consecutive epochs. The training stopped if the validation loss did not decrease for 10 consecutive epochs. Tables 1 and 2 show the results of the proposed VGTL method and the comparison method from Dall'Olio *et al.* [10]. Observe that the VGTL outperformed the comparison method in both multiclass and binary classification problems. For the multiclass classification problem, VGTL converged much

faster than the comparison method. Figures 10 and 11 show the confusion matrices for the multiclass and binary classification problems of one of the train/validation/test splits.

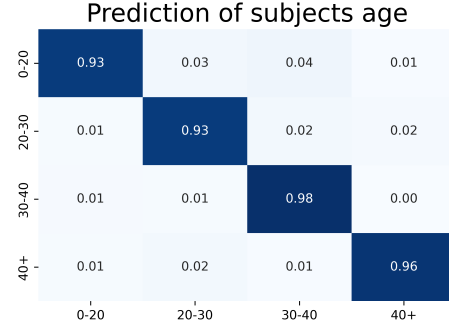


Fig. 10: The confusion matrix of the performance of the VGTL on the four-class classification task.

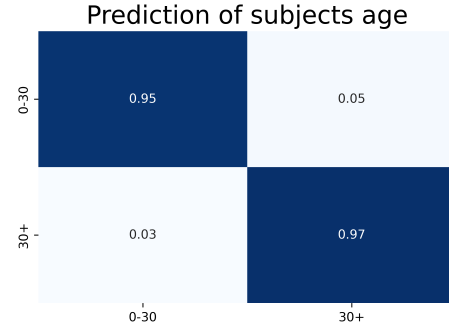


Fig. 11: The confusion matrix of the performance of the VGTL on the binary classification task.

In the regression task, the proposed VGTL model demonstrated a high performance from the perspective of average mean absolute error and standard deviation, with values of 1.41 years and 0.14 years, respectively. Figure 12 shows the predicted age and ground truth age of subjects in the test set. To the best of our knowledge, this is the first study to perform regression on subjects' age for comparison.

For the preprocessing part, the method proposed by Dall'Olio *et al.* [10] firstly removed the trend of the PPG signal using a centered moving average. The processed PPG signal was then demodulated using a Hilbert transform and the envelope was extracted. The final version of the PPG signal was obtained by dividing the demodulated signal by the envelope. In contrast, our method did not require any preprocessing and simply used a **findpeaks** function in **MATLAB**. In addition, both methods used deep learning to classify the age group. The comparison method adapted the ResNet model from the computer vision area to work for one-dimensional signals. On the other hand, our method

is naturally suitable for convolutional neural networks for two-dimensional images, which motivates and enables us to utilise the power of transfer learning, thus resulting in faster convergence and better performance. Overall, our proposed VGTL showed advantages in both preprocessing and learning, as VGTL required much less preprocessing and did not require complex human-designed and dataset-oriented rules. Moreover, the VGTL method could easily convert a 1D signal into a 2D signal, which makes it suitable to utilise powerful CNNs and transfer learning.

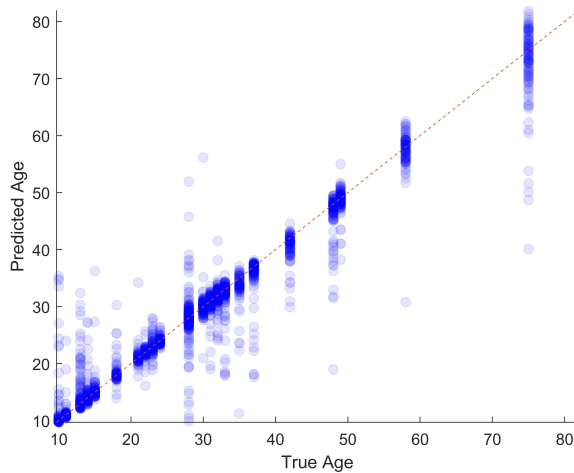


Fig. 12: The results of age prediction vs the ground truth age of the subjects in the test set.

3.2. Blood Pressure Estimation.

3.2.1. Dataset

The dataset used was a processed version of the MIMICII [18]. The 0-0.25 Hz and 250-500 Hz components were removed from the raw PPG signals through wavelet decomposition. Then, the filtered PPG signals were soft thresholded and reconstructed [18]. In total, 1000 records were selected according to the computation resources available. There might be more than one record per patient.

3.2.2. Aim and Goal

The aim of this experiment was to predict a blood pressure waveform from the PPG signal. To this end, a PPG signal was fed into the model and a blood pressure waveform of the same length (in seconds) was generated. Next, the systolic blood pressure (SBP) and diastolic blood pressure (DBP) were extracted and compared to the ground truth.

3.2.3. Data Preparation and Model Architecture

A plateau detection procedure was applied to the PPG signals and any segments found to contain a plateau were subsequently removed from the dataset. No further preprocessing was performed. Both the PPG signal and blood pressure signal had sampling rates of 125 Hz, and they were segmented into windows of length 224, corresponding to the default input size of VGG19 (224x224). The first two channels were the adjacency matrices of the visibility graphs generated from the PPG signal and the inverted PPG signal. The third channel was the adjacency matrix of a slope-weighted visibility graph generated from the inverted PPG signal. The output top layer for this experiment was an MLP of size (1000x224) with no activation function.

3.2.4. Results and Discussion

Figure 13 shows two examples of predicting the blood pressure waveform from PPG signal segments. Observe that the predicted blood pressure waveforms were close to the ground truth blood pressure waveforms. As for the prediction of SBP and DBP, Table 3 presents the test results of VGTL and the British Hypertension Society blood pressure measurement grading system. Our method could achieve Level A for DBP estimation and Level C for SBP estimation. As for the waveform prediction, the VGTL could reach an average mean absolute error of 5.62 mmHg. It is important to mention that the quality of this dataset is severely undermined by the fact that the MIMICII dataset was recorded on patients in critical conditions, with poor instrumentation and signal qualities, which affected the performance. Figure 14 shows exemplar blood pressure predictions with undermined ground truth blood pressure signals. Note that our method gave reasonable blood pressure waveform predictions when the blood pressure reference waveform showed significant measurement errors. Furthermore, considering that the quality of the dataset may not be optimal, the performance of our proposed algorithm could potentially be improved. There may be room for further enhancement in the effectiveness of the algorithm as the data quality improves. To the best of our knowledge, this is the first work that is capable predict the blood pressure waveform continuously. This demonstrates that VGTL was able not only to analyse the structural information from the PPG signal but also to extract magnitude values from pure structural information. The VGTL algorithm was also fast, with an average execution time of 0.625 milliseconds for every PPG segment of 1.792 seconds long. Moreover, the only preprocessing required was plateau detecting, which again indicated the low preprocessing requirement of VGTL.

4. DISCUSSIONS

We have proposed a novel model called Visibility Graph and Transfer Learning (VGTL) that combines graph theory, com-

Method	Accuracy: Four Classes	Epochs
VGTL	$97.20 \pm 0.2393\%$	26.66 ± 3
Dall’Olio, et al.	87.14%	280

Table 1: Multiclass classification performances of VGTL and the method in [10].

Method	Accuracy: Binary Classes	Epochs
VGTL	$95.7 \pm 0.1375\%$	22 ± 1.35
Dall’Olio, et al.	95.3%	Not Known

Table 2: Binary classification performances of VGTL and the method in [10].

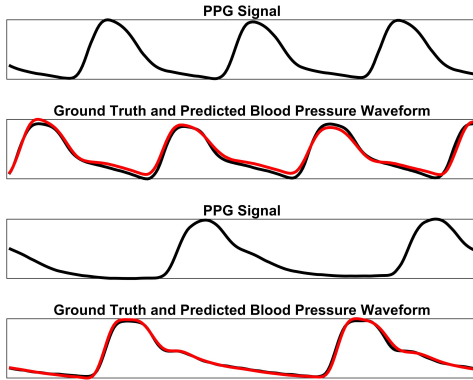


Fig. 13: Two examples of predicting the blood pressure waveform using VGTL from PPG signal segments. The red lines denote the predicted blood pressure waveform and the black lines represent the ground truth.

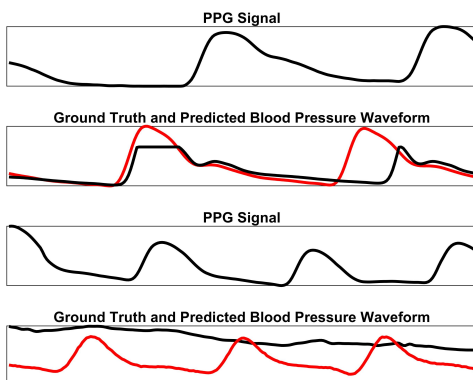


Fig. 14: Three examples of predicting blood pressure waveform using VGTL when the ground truth blood pressure segments are of bad qualities. The red lines denote the predicted blood pressure waveform and the black lines designate the ground truth.

puter vision and deep learning to analyse photoplethysmography (PPG) signals. The method first converts the signals to visibility graphs and represents them as adjacency matrices that can easily be visualised as images. This transforms the one-dimensional PPG signals into their two-dimensional representations, which are suitable as inputs to convolutional networks. We have demonstrated that visibility graphs can capture the physiological characteristics of their adjacency matrices, which underpins the VGTL model. Moreover, the affine transformation invariant property of the visibility graph makes it robust for PPG signals that are constantly affected by baseline wandering and motion artefacts. The visibility graph only preserves the structural information and discards the magnitude information, which is advantageous since the magnitude is influenced by many factors, such as age, and could be misleading. After extracting the adjacency matrices as images, we apply the VGG19 model, a transfer learning algorithm, to these images to produce the final output. This enables one-dimensional PPG signals to leverage the power of computer vision algorithms that only work on two-dimensional images.

We have tested the VGTL model on the prediction of the subjects’ age and blood pressure from pure PPG signals, and it has shown its powerful generalisation abilities by performing classification and regression on two different tasks and two different datasets. The VGTL model has demonstrated its advantage of requiring fewer preprocessing steps, and the absence of any requirement to apply algorithms such as principal component analysis (PCA) to retrieve information or empirical mode decomposition (EMD) to single out signal components. This makes the model more robust and easier to apply since many of the preprocessing algorithms are sensitive to parameters and require human calibration. Other advantages of VGTL are the elimination of manually extracting features from PPG signals, as the PPG signals are fed to the VGTL model as a whole. This is critically important for signals with low quality that might affect feature extraction algorithms.

In summary, the VGTL algorithm provides a simple yet powerful framework that has good generalisation ability, and has the potential to become a universal framework that is suit-

Grade	Absolute Difference between the Standard and Test Device (%)		
	$\leq 5 \text{ mmHg}$	$\leq 10 \text{ mmHg}$	$\leq 15 \text{ mmHg}$
A	80	90	95
B	65	85	95
C	45	75	90
D	Worse than C		
VGTL (DBP)	83.93	96.03	98.77
VGTL (SBP)	48.87	75.87	88.40

Table 3: The British Hypertension Society standard (BHS) and the VGTL results.

able for multiple applications.

5. REFERENCES

- [1] H. J. Davies, I. Williams, G. Hammour, M. Yarici, M. J. Stacey, B. M. Seemungal, and D. P. Mandic, “In-ear spo₂ for classification of cognitive workload,” *IEEE Transactions on Cognitive and Developmental Systems*, pp. 1–1, 2022.
- [2] W.-K. Beh, Y.-H. Wu, and A.-Y. Wu, “Robust ppg-based mental workload assessment system using wearable devices,” *IEEE Journal of Biomedical and Health Informatics*, vol. 27, no. 5, pp. 2323–2333, 2023.
- [3] G. Hammour and D. P. Mandic, “An in-ear ppg-based blood glucose monitor: A proof-of-concept study,” *Sensors*, vol. 23, no. 6, p. 3319, 2023.
- [4] C. Zhang, E. Jovanov, H. Liao, Y.-T. Zhang, B. Lo, Y. Zhang, and C. Guan, “Video based cocktail causal container for blood pressure classification and blood glucose prediction,” *IEEE Journal of Biomedical and Health Informatics*, vol. 27, no. 2, pp. 1118–1128, 2023.
- [5] H. J. Davies, P. Bachtiger, I. Williams, P. L. Molyneaux, N. S. Peters, and D. P. Mandic, “Wearable in-ear PPG: Detailed respiratory variations enable classification of COPD,” *IEEE Transactions on Biomedical Engineering*, vol. 69, no. 7, pp. 2390–2400, 2022.
- [6] K. V. Madhav, M. R. Ram, E. H. Krishna, N. R. Kollama, and K. A. Reddy, “Robust extraction of respiratory activity from PPG signals using modified MSPCA,” *IEEE Transactions on Instrumentation and Measurement*, vol. 62, no. 5, pp. 1094–1106, 2013.
- [7] B. Prathyusha, T. S. Rao, and D. Asha, “Extraction of respiratory rate from PPG signals using PCA and EMD,” *International Journal of Research in Engineering and Technology*, vol. 1, no. 2, pp. 164–184, 2012.
- [8] M. R. Ram, K. V. Madhav, E. H. Krishna, N. R. Kollama, K. Sivani, and K. A. Reddy, “ICA-based improved DTCWT technique for MA reduction in ppg signals with restored respiratory information,” *IEEE Transactions on Instrumentation and Measurement*, vol. 62, no. 10, pp. 2639–2651, 2013.
- [9] M. A. Motin, C. K. Karmakar, and M. Palaniswami, “Selection of empirical mode decomposition techniques for extracting breathing rate from PPG,” *IEEE Signal Processing Letters*, vol. 26, no. 4, pp. 592–596, 2019.
- [10] L. Dall’Olio, N. Curti, D. Remondini, Y. Safi Harb, F. W. Asselbergs, G. Castellani, and H.-W. Uh, “Prediction of vascular aging based on smartphone acquired PPG signals,” *Scientific reports*, vol. 10, no. 1, pp. 1–10, 2020.
- [11] S. Suzuki and K. Oguri, “Cuffless blood pressure estimation by error-correcting output coding method based on an aggregation of Adaboost with a photoplethysmograph sensor,” *Proceedings of the Annual International Conference of the IEEE Engineering in Medicine and Biology Society*, pp. 6765–6768, 2009.
- [12] L. Lacasa, B. Luque, F. Ballesteros, J. Luque, and J. C. Nuno, “From time series to complex networks: The visibility graph,” *Proceedings of the National Academy of Sciences*, vol. 105, no. 13, pp. 4972–4975, 2008.
- [13] M. A. Pimentel, P. H. Charlton, and D. A. Clifton, “Probabilistic estimation of respiratory rate from wearable sensors,” in *Wearable Electronics Sensors*. Springer, 2015, pp. 241–262.
- [14] Q. Yousef, M. Reaz, and M. A. M. Ali, “The analysis of PPG morphology: Investigating the effects of aging on arterial compliance,” *Measurement Science Review*, vol. 12, no. 6, p. 266, 2012.
- [15] C. Tan, F. Sun, T. Kong, W. Zhang, C. Yang, and C. Liu, “A survey on deep transfer learning,” *Proceedings of the International Conference on Artificial Neural Networks*, vol. 11141, pp. 270–279, 2018.
- [16] J. Deng, W. Dong, R. Socher, L.-J. Li, K. Li, and L. Fei-Fei, “Imagenet: A large-scale hierarchical image database,” *Proceedings of the IEEE Conference on Computer Vision and Pattern Recognition*, pp. 248–255, 2009.
- [17] A. Siam, “Real-World PPG dataset,” 2019.
- [18] M. Kachuee, M. M. Kiani, H. Mohammadzade, and M. Shabany, “Cuffless blood pressure estimation algorithms for continuous health-care monitoring,” *IEEE Transactions on Biomedical Engineering*, vol. 64, no. 4, pp. 859–869, 2016.